Investigations into the effects of volatile biomass tar on the performance of Fe-based CLC oxygen carrier materials

2016 Environ. Res. Lett. 11 115001

(http://iopscience.iop.org/1748-9326/11/11/115001)

Environmental Research Letters

LETTER

Investigations into the effects of volatile biomass tar on the performance of Fe-based CLC oxygen carrier materials

Matthew E Boot-Handford[1], **Nick Florin**[2,3] **and Paul S Fennell**[1]

[1] Department of Chemical Engineering, Imperial College London, SW7 2AZ, London
[2] Grantham Institute for Climate Change, Imperial College London, SW7 2AZ, London
[3] Institute for Sustainable Futures, University of Technology Sydney, NSW 2007, Austalia

E-mail: p.fennell@imperial.ac.uk

Keywords: chemical-looping combustion, biomass, tar, chemical-looping reforming, bio-syngas upgrading, BECCS

Supplementary material for this article is available online

OPEN ACCESS

RECEIVED
11 February 2016

REVISED
15 August 2016

ACCEPTED FOR PUBLICATION
12 September 2016

PUBLISHED
25 October 2016

Abstract

In this study we present findings from investigations into interactions between biomass tar and two iron based oxygen carrier materials (OCMs) designed for chemical-looping applications: a 100% Fe_2O_3 (100Fe) OCM and a 60 wt% Fe_2O_3/40 wt% Al_2O_3 (60Fe40Al) OCM. A novel 6 kW_e two-stage, fixed-bed reactor was designed and constructed to simulate a chemical-looping combustion (CLC) process with *ex situ* gasification of biomass. Beech wood was pyrolysed in the first stage of the reactor at 773 K to produce a tar-containing fuel gas that was used to reduce the OCM loaded into the 2nd stage at 973 K. The presence of either OCM was found to significantly reduce the amount of biomass tars exiting the reactor by up to 71 wt% compared with analogous experiments in which the biomass tar compounds were exposed to an inert bed of sand. The tar cracking effect of the 60Fe40Al OCM was slightly greater than the 100Fe OCM although the reduction in the tar yield was roughly equivalent to the increase in carbon deposition observed for the 60Fe40Al OCM compared with the 100Fe OCM. In both cases, the tar cracking effect of the OCMs appeared to be independent of the oxidation state in which the OCM was exposed to the volatile biomass pyrolysis products (i.e. Fe_2O_3 or Fe_3O_4). Exposing the pyrolysis vapours to the OCMs in their oxidised (Fe_2O_3) form favoured the production of CO_2. The production of CO was favoured when the OCMs were in their reduced (Fe_3O_4) form. Carbon deposition was removed in the subsequent oxidation phase with no obvious deleterious effects on the reactivity in subsequent CLC cycles with reduction by 3 mol% CO.

1. Introduction

Development of a commercially viable carbon capture and sequestration (CCS) technology for fossil fuel power generation is necessary to avoid anthropogenic climate change [1, 2]. Chemical-looping combustion (CLC) is an indirect combustion process that utilises a regenerable solid oxygen sorbent (oxygen carrier (OC) material, OCM), typically a metal oxide, to transfer oxygen from the combustion air to the fuel such that direct contact between air and fuel is avoided [3–6]. CLC is a variant on an oxy-fuel carbon capture system that offers the potential for a much lower energy penalty as CO_2 separation is achieved intrinsically such that additional energy-intensive gas separation steps are avoided [7].

To date, research efforts have predominantly focused on the development of a CLC technology using fossil fuels such as natural gas [4, 8–11], coal [12–17] and pet coke [18–20]; however over the last few years there has been growing interest in the application of CLC technology for biomass utilisation [21–25]. Bioenergy-CCS (BECCS) processes are of particular interest as they have the potential to result in negative CO_2 emissions i.e. a net removal of CO_2 from the atmosphere and represent one of the most efficient and cost-effect methods for doing so [1, 26]. Negative emissions technologies will be necessary if mitigation

efforts continue to fall short of targets and atmospheric greenhouse gas concentrations remain on an increasing trajectory towards stabilisation at dangerous levels [1].

Gasification of biomass typically produces substantial quantities of refractory tar compounds. Tar is difficult to combust in a chemical-looping system (gaseous oxygen is not necessarily present in the fuel reactor; the temperature may also be limited by endothermic gasification and chemical-looping fuel oxidation reactions) which can lead to reduced fuel conversion efficiencies [27]. Decomposition of tars on the surface of the OCM can result in severe coking and temporary deactivation. Coking also hinders the overall CO_2 capture efficiency of the process as regeneration of the OCM in air produces CO_2 which cannot be captured [27, 28].

A few research groups have now tested the use of biomass in interconnected dual fluidised bed CLC systems with *in situ* gasification and combustion of the biomass [22, 29]. Mendiara *et al* [25] studied the CLC of sawdust in a 500 kW_{th} interconnected fluidised bed CLC unit with hematite as the OC. They achieved carbon capture efficiencies of >95% at temperatures between 1053–1188 K using steam and CO_2 as the gasifying agents. The tar content of the gas stream exiting the fuel reactor was 0.2–1.38 g Nm^{-3}, which requires additional clean-up prior to CO_2 pipeline entry. Despite this, the tar destruction efficiency of the CLC process using hematite was ~5 times greater than that for similar experiments with a Fe/olivine tar cracking catalyst. The authors attributed the improved tar cracking efficiency of the CLC process to the ability of the hematite to react with tar rather than solely acting as a catalyst.

A large proportion of biomass/CLC research has focused on the development of bio-syngas upgrading/tar removal systems [24, 30, 31]. Larsson *et al* [32] studied ilmenite as a tar cracking catalyst to upgrade biosyngas from gasification of woody biomass in a 2–4 MW_{th} interconnected fluidized bed system. Adding small (~12 wt%) amounts of ilmenite to a solids inventory of sand reduced the tar yield by ~50 wt%, but reduced the cold gas efficiency by 10%. A similar earlier study using the same reactor found that ilmenite was less effective resulting in a reduction in the amount of tar exiting the process of 35% for a residence time of 0.4–0.5 s with a raw gas feed containing 30 g Nm^{-3} of tar [33]. The resulting (detectable) tar species were found to consist of predominantly stable ring structures such as benzenes and napthalenes.

Lind *et al* [34] compared tar cracking capabilities of ilmenite and a synthetic Al_2O_3 supported NiO OCM in a chemical-looping reforming (CLR) process. The Ni-based OCM resulted in >95% reduction in the tar content of the outlet gas compared with 60% for the ilmentite catalyst at 1153 K and 1123 K respectively. Both materials were affected by small amounts of carbon deposition but no lasting effects on the reactivity after regeneration in the air reactor were observed. Carbon deposition was kept low (<0.25%) by maintaining a high solid circulation rate between the fuel and air reactors.

This paper presents findings from investigations into the effect of tars produced from biomass pyrolysis on the performance of two iron-based CLC OC materials (OCMs) (a pure Fe_2O_3 OCM and an OCM consisting of 60 wt% Fe_2O_3 supported with 40 wt% Al_2O_3). It makes use of a two-stage fixed-bed reactor, specifically designed for studying interactions between pyrolysis (or gasification) tar and OCMs for CLC processes. The conditions were tailored such that the tar content of the fuel gas was much larger than what would be expected in a commercial process, to accelerate potential degradation of the OCMs and enable more ready analysis. Furthermore, the use of large quantities of tars meant that appreciable amounts of tar could be collected after exposure to the OCMs for analysis. Previous work involving the use of biomass as a fuel for CLC processes demonstrates that improved tar cracking capabilities of OCMs to reduce the amount of tar exiting the process is necessary for CO_2 pipeline entry and improved overall process efficiency.

2. Experimental

2.1. Reactor

A 6 kW_e, 2-stage fixed-bed reactor was designed and constructed, based on an update and upgrade of an existing reactor [35–38]. A number of limitations, were overcome, namely: (i) welded flange connections were replaced with twin-ferrule compression fittings to allow for operation at pressures up to 30 bar_a and temperatures up to 1273 K; (ii) the reactor has a wider internal diameter to allow for solid fuel feeding during operation; (iii) inert quartz tubes incorporating sintered quartz disks, acting as bed supports, lined the inside of the reactor to prevent undesirable reactions between gaseous reactants and products with the potentially catalytically active reactor walls [39]; (iv) a new tar trap (described below) was designed to enable efficient tar trapping with an ice and salt water coolant as opposed to liquid N_2—this means that N_2 could be used as the carrier gas instead of He, and CO_2 and steam could be introduced as a reactive gas.

The reactor could be operated in a two-stage (figure 1) or single-stage configuration (not shown). The body was an Incoloy 800HT pipe (25.4 mm ID, 3.8 mm wall thickness). The first or single stage was 350 mm in length and contained only a single bed (i.e. the top section of the 2-stage reactor depicted in figure 1). For 2-stage operation, the reactor was 600 mm in length. A compression fitting at the top of the reactor provided the pressure sealed connection for the gas inlet, solid fuel feeder and 1st stage thermocouples; a similar fitting at the base of the reactor

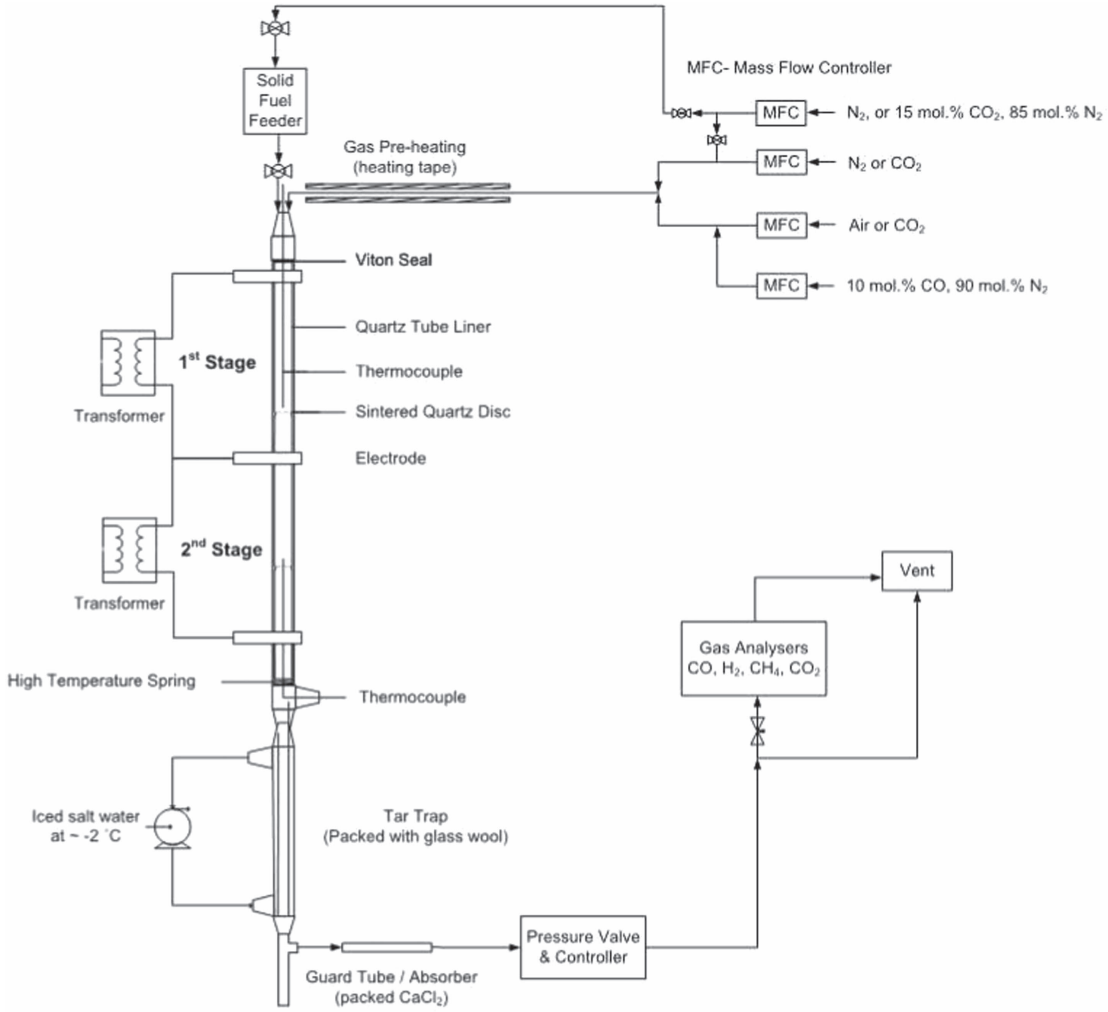

Figure 1. Schematic diagram of the new two-stage, fixed-bed reactor.

provided the connection to the tar trap and 2nd stage thermocouples.

Biomass samples were fed into the first stage of the reactor batch-wise. The feeder was a 50 ml stainless steel sample vessel with ball valves at the inlet and outlet. A ¼ inch (4.6 mm ID, 0.9 mm wall thickness) stainless steel tube provided the pathway for the biomass sample into the reactor ensuring that all of the sample was fed onto the 1st stage bed support.

Mass flow controllers (Bronkhorst High-Tech B.V.) controlled and monitored the flow rate and composition of the gas entering the reactor, for fast and accurate gas switching. Pressure was controlled and monitored by a pressure controller and pneumatic valve (Bronkhorst High-Tech B.V.) at the exit of the tar trap.

Inert quartz tubes incorporating sintered quartz disks, which acted as the bed supports lined the inside of the reactor. A Viton seal at the top of the quartz tube prevented gas bypass. A bespoke high-temperature Inconel spring situated at the base of the quartz tube provided the force for sealing and compensated for reactor length changes from thermal expansion.

Depending on the operating conditions and gases used, the fuel could be pyrolysed, gasified or combusted in the 1st stage generating a fuel or exhaust gas for directly analysis (single-stage experiments) or further reaction in the 2nd stage. Ash and residual char was retained on the sintered quartz disk in the first stage and the evolved gases and volatiles were swept downstream into the tar trap or 2nd stage. The 2-stage configuration utilised a bed of either the OCMs or sand that were pre-loaded into the 2nd stage. The effects of these different solid particles on the fuel/exhaust gases could then be determined by comparison with the results obtained from single-stage experiments.

The single stage reactor was heated via two copper electrodes that were attached to the outside, at the top and bottom of the reactor body. The reactor body acted as a resistance heater. The 2-stage reactor was heated via three electrodes with a central bridging electrode (figure 1). The electrode that attached to the top of the 1st stage was rigid and acted as a support for the reactor. The other electrodes were attached to the reactor with flexible copper cables to allow for thermal expansion of the reactor body. All the electrodes were water-cooled. The two stages were heated using separate controllers and transformers enabling operation at different temperatures.

Table 1. Summary of experimental operating parameters carried out in the 2-stage fixed bed reactor with biomass pyrolysis in the first stage.

Operating conditions	1st stage	2nd stage
Biomass feedstock	Beech wood (0.100 g, d_p = 106–150 μm)	N/A
2nd stage bed material	N/A	Sand 100Fe OCM 60Fe40Al OCM (0.750 g, 300–425 μm)
Temperature	773 K	973 K
Pressure	1.5 bar_a	
Superficial velocity (1st stage/2nd stage)	0.25 m s^{-1}, 0.40 m s^{-1}	
Reduction phase[c]	3% CO/15% CO_2/82% N_2 (300 s)	
Oxidation phase[c]	4% O_2/96% N_2 (300 s)	
Purge phase[c]	100% N_2 (120 s)	
Total number of cycles	5 (or 3 ended after the biomass pyrolysis phase)	
Biomass pyrolysis cycle no.	3	
Conditions of biomass pyrolysis	100% N_2 PreRed[a] 100% N_2 PostRed[b] 15% CO_2 PreRed 15% CO_2 PostRed	

[a] Pre-Red refers to experiments where the biomass pyrolysis phase is carried out before a gaseous reduction phase.
[b] Post-Red refers to experiments where the biomass pyrolysis phase is carried out after a gaseous reduction phase.
[c] Gas compositions are presented on a mole basis.

The tar trap design was an annular heat-exchanger consisting of a 1000 mm long, ½ inch OD (10.4 mm ID, 1.1 mm wall thickness) stainless steel inner tube with a 1 inch OD (21.2 mm ID, 2.1 mm wall thickness) outer tube connected around the outside of the ½ inch tube with 2 × 1 inch T-piece Swagelok connections. The gas exited the reactor through the internal ½ inch tube. The trap was cooled to ~270 K by pumping iced salt water around the annulus of the tar trap. The exit of the trap was loosely packed with ~6 g of glass wool to increase the internal surface area ensuring efficient trapping of the tars vapours in the form of aerosol droplets. The concentrations of CO_2, CO and CH_4 in the gas stream exiting the reactor were measured using online infrared analysers (ADC MGA 3000, 0–50 mol-% ± 1% of the measured value) connected after the pressure control valve. A thermal conductivity H_2 analyser (Hi-Tech K1500) was also installed but H_2 was not detected in any experiments.

Operation of the reactor was automated where appropriate using a control programme written in Agilent Vee, which controlled setpoints and monitored and collected data (logged every second) associated with fuel feeding, temperature, pressure, flow rates and gas analyser outputs.

2.2. Materials

Two OCMs were investigated: 100 wt% Fe_2O_3 (100Fe) and 60 wt% Fe_2O_3 supported by 40 wt% Al_2O_3 (60Fe40Al). The OCMs were prepared via simple mechanical mixing and pelletisation. Stoichiometric quantities of the precursor powders, Fe_2O_3 (<5 μm, *Sigma Aldrich*) and $Al(OH)_3$ (*Sigma Aldrich*) were added to a high shear mini-mixer (50 g capacity, *Caleva Solutions Ltd*) and dry mixed for 30 min to ensure the powders were well combined. Deionised water was added dropwise until an extrudable paste had formed, which was extruded through a 425 μm sieve. The extrudates were converted to spherical particles using a spheronizer (*Caleva Solutions Ltd*) and then sintered in a horizontal tube furnace for 4 h under a constant air purge. The 100Fe OCM particles were sintered at 1173 K and the 60Fe40Al OCM particles were sintered at 1273 K.

Beech wood was the sole biomass variety used in this study. Samples were first ground in a high-shear cutting mill then sieved to obtain a size fraction of 106–150 μm and finally dried in an air-circulating oven at 308 K for 16 h to remove the free moisture.

2.3. Operating conditions

A standard set of conditions were developed and used when operating the single-stage reactor (summarised in table 1). 2.8 g of sand (David Ball; sieved to 300–425 μm) was loaded into the first stage to provide a small inert bed (5 mm in height) that the 1st stage bed thermocouple could be submerged in. Sand has a high thermal capacity and provided a stable heat sink, allowing stable and precise measurement and control of the 1st stage bed temperature. The 2nd stage bed (if used) was either loaded with 0.75 g of sand (300–425 μm) or 0.75 g of an OCM material (100Fe or 60Fe40Al, 300–425 μm).

Once the reactor was assembled, a cold calibration was performed using a certified calibration gas mixture (29.9 mol% CO_2, 9.7 mol% CO, 10.1 mol% CH_4, balance N_2) supplied by BOC. For the experiments involving fast pyrolysis of the beech wood in 15 mol% CO_2 (balance N_2) and 3 mol% CO, 15 mol% CO_2 (balance N_2), two cold blank cycles with a simulated biomass feed (i.e. empty feed vessel) were performed to establish a baseline concentration profile that could be used for data analysis and determining the final pyrolysis product distribution. A total flow rate of 60 $ml_N\ s^{-1}$ was used, equivalent to superficial velocities of 0.25 m s^{-1} and 0.40 m s^{-1} through the 1st and 2nd stages at 773 K and 973 K respectively. Gas was supplied from BOC gas cylinders of (i) pure CO_2, (ii) 10 mol% CO, balance N_2 and (iii) pure N_2; (iv) laboratory air was also supplied.

The reactor was heated to the setpoint temperatures. When temperatures were stable, the tar trap cooling system was switched on and the beech wood (0.1 g, 106–150 μm) was loaded into the feed vessel. The tar trap was allowed to cool for 15 min and the feed vessel was purged (10 $ml_N\ s^{-1}$) for at least 10 min before starting an experiment. A flow of 15 mol% CO_2, 85 mol% N_2 (certified premixed gas mixture supplied by BOC) was used for purging the feed vessel and pressure feeding the biomass for experiments in which 15 mol% CO_2 was introduced into the inlet gas to minimise disruptions in the CO_2 concentration profile.

When using OCMs in the 2nd stage, the OCMs first needed to be activated by performing 2 simulated CLC cycles [40]. A simulated CLC cycle consisted of a 300 s reduction phase (15 mol% CO_2, 3 mol% CO, 82 mol% N_2) and a 300 s oxidation phase (4 mol% O_2, 96 mol% N_2) separated by two 120 s phases in which the reactor was purged with N_2. These conditions have been used elsewhere for the investigation of Fe-based OCM reduction kinetics and cycling performance testing [41, 42]. The activation CLC cycles were unnecessary for single-stage experiments or when the 2nd stage was loaded with sand. Biomass feeding was initiated once a stable target inlet gas composition had been reached. Biomass was fed by pressuring the sample feed vessel to 0.5 bar above the setpoint pressure of the reactor and then opening both valves to force the biomass sample into the first stage of the reactor.

Interactions between the OCMs and the volatile biomass pyrolysis products were investigated under two different inlet gas compositions: (i) 100% N_2 and; (ii) 15 mol% CO_2, 85 mol% N_2. When biomass pyrolysis was carried out under 100% N_2, no thermodynamic limitation on the final oxidation state of the OCM was imposed such that the OCM could have been reduced further than Fe_3O_4. The addition of 15 mol% CO_2 into the inlet gas controlled the final reduction state of the 100Fe OCM to Fe_3O_4 (based on the assumption of a simplified system involving CO, CO_2 and N_2 only and providing the concentration of CO in the reactor did not exceed 9.4 mol% at 973 K, see phase equilibrium diagram, figure S1). Biomass was fed into the reactor either before the 3rd cycle reduction (PreRed) or after the 3rd cycle reduction (PostRed) to investigate interactions between the OCM in its oxidised (Fe_2O_3) or reduced (Fe_3O_4) forms respectively.

Experiments were either ended immediately after the biomass pyrolysis phase to allow for retrieval of the OCM particles directly after exposure to the pyrolysis vapours; or continued such that another 2 complete cycles (gaseous reduction with 3 mol% CO, 15 mol% CO_2, balance N_2) were completed with the aim of establishing whether exposure to the volatile pyrolysis products affected the reactivity of the OCM in subsequent redox cycles. A higher O_2 concentration of 10 mol% was needed for the 3rd cycle oxidation phase after the biomass pyrolysis to ensure that the char bed remaining in the 1st stage was completely burnt off.

Table 2. Summary of N_2 adsorption and mercury intrusion porosimetry (MIP) measurements obtained for the different Fe_2O_3-based OC particles prepared in this study.

	100Fe	60Fe40Al
Surface area ($m^2\ g^{-1}$)	1.06	28.96
Cumulative vol. of pores (1.7–300 nm) ($cm^3\ g^{-1}$)	0.017	0.213
Average pore size (1.7–300 nm) (nm)	105	28
Cumulative volume of pores (0.05–10 μm) ($cm^3\ g^{-1}$)	0.15	0.47
Average pore diameter 4 V A^{-1} (0.05–10 μm) (nm)	551	65
Skeletal density $\times\ 10^{-6}$ ($g\ m^{-3}$)	4.00	4.83
Porosity (0.05–10 μm)	0.37	0.69
Envelope density $\times\ 10^{-6}$ (0.05–10 μm) ($g\ m^{-3}$)	2.52	1.48

2.4. Product recovery

After each experiment, the reactor was dismantled and each of the reactor components was carefully washed with a 4:1 (v/v) solution of chloroform and methanol (150 ml) to recover tars. The washings were filtered using filter paper (Whatman, grade 5) to collect solids. The bulk of the solvent was removed by evaporation on a rotary evaporator (BUCHI-R210) at conditions of 333 K, 0.337 bar and 40 rpm until most of the solvent was evaporated. The tar was then transferred to an aluminium beaker and placed in a N_2-purged oven at 308 K for 2 h to evaporate residual solvent. The tar was then weighed to determine the gravimetric yield. Char yields were determined according to the method outlined in section S.1. All error ranges provided in the figures below are presented as a single standard deviation from the mean. Unless specifically stated otherwise, all data points are presented with an associated error range of a single standard deviation on either side of the mean.

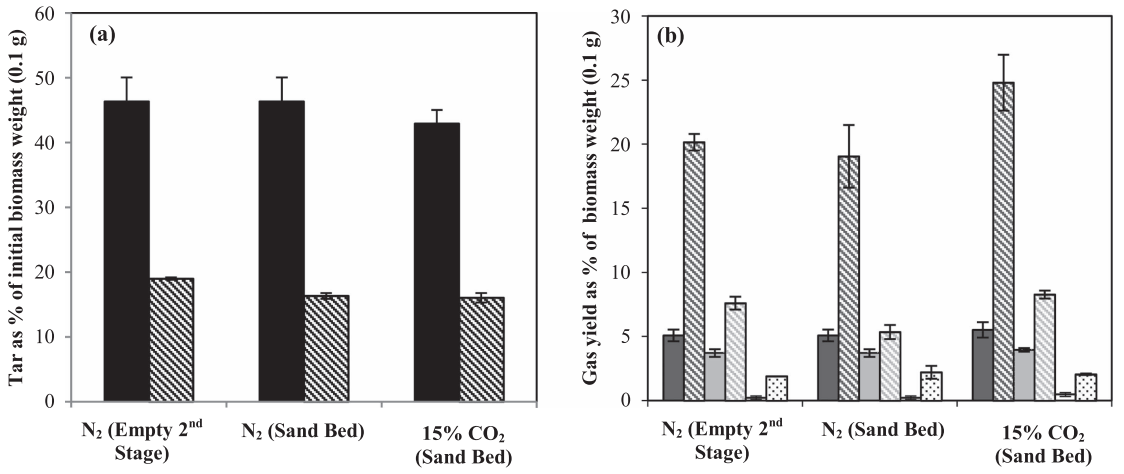

Figure 2. (a) Tar yields and (b) detectable gas yields produced from the fast pyrolysis of 0.100 g of beech wood in different gaseous environments in the single-stage (filled bars) and two-stage reactor at 973 K (pattern filled bars) with and without a sand bed in the 2nd reactor stage. Tar (black bars), CO (dark grey bars), CO_2 (light grey bars) and CH_4 (white/polka dot filled bars).

2.5. Product characterisation

Size exclusion chromatography (SEC) (for the molecular size distribution) was used to characterise the tars (method outlined in section S.2) [43].

N_2-adsorption analysis (Micrometrics, Tristar 3000) was carried out to determine the BET surface area and BJH pore size distributions of the fresh, unreacted OCMs for the pore size range 2–200 nm. The size distribution and volume of pores in the pore size range 5–10000 nm was achieved using mercury porosimetry (Micrometrics Autopore IV). A summary of the morphological characteristics of the two OCMs is provided in table 2.

3. Results and discussion

Results from the single-stage pyrolysis experiments indicate that the inlet gas composition had little influence on the primary pyrolysis product distribution (figure 2). Tar yields were 42.9 wt% and 46.3 wt%; and char yields were between 20.3 wt% and 23.0 wt% experiments carried out in atmospheres containing 100 mol% N_2, and 15 mol% CO_2, (bal. N_2) respectively. Variation was within the experimental error of the measurements. This was to be expected as the temperature of the first stage (i.e. 773 K) was too low for gasification reactions between the pyrolysis products and CO_2 introduced in the inlet to take place at a fast enough rate to cause noticeable differences in the product distribution [44].

Subjecting the tar and other volatile pyrolysis products produced in the first stage to the 2nd stage at an elevated temperature of 973 K caused a substantial reduction in the tar yield (figure 2(a)). The reduction in the tar yield was accompanied by a significant increase in the yield of CO and a smaller increase in the CO_2 yield. An inert sand bed in the 2nd stage modestly reduced the tar yield further, without significantly affecting the gas yields. The tar yield was not affected by 15% CO_2 in the carrier gas, though slightly improved yields of CO and CO_2 were observed, attributed to gasification reactions between the CO_2 in the carrier gas and undetected pyrolysis products such as light hydrocarbons and carbon deposits.

Exposure of the pyrolysis products to the bed of 100Fe OCM in the 2nd stage, as opposed to an inert sand bed, caused an additional reduction in tar yield (figure 3) of between 26.7 and 38.9 wt%. The amount of tar recovered after exposure to the 100Fe bed in both its oxidised and reduced forms under the different gaseous environments was between 10.1 and 11.8 wt%. No distinguishable trend was observed between tar yield and the condition of the OC or inlet gas composition.

A larger reduction (relative to the 100Fe OCM) in the tar yield was observed when the pyrolysis products were exposed to the 60Fe40Al OCM in the 2nd stage, of 48–71 wt%, most likely from enhanced oxidation, gasification and cracking on the substantially larger surface area of the 60Fe40Al (table 2).

SEC analysis of the retrieved tar (figure 4) demonstrated subtle differences in the molecular mass distribution of the tar collected after exposure to both the 100Fe and 60Fe40Al OCMs in their oxidised (Fe_2O_3) and reduced (Fe_3O_4) forms. The tar recovered after exposure to the reduced OCMs (i.e. 'PostRed' conditions) appeared to comprise of a larger proportion of the higher molecular mass fraction (excluded peak) and less of the lower molecular mass fraction (retained peak) compared with the tar recovered after exposure to the oxidised OCMs ('PreRed' conditions). The same trends in the SEC analysis were observed for the tar recovered after analogous experiments in an atmosphere of 15 mol% CO_2, balance N_2 (figure S.3). The SEC results indicate that the oxidation state of the

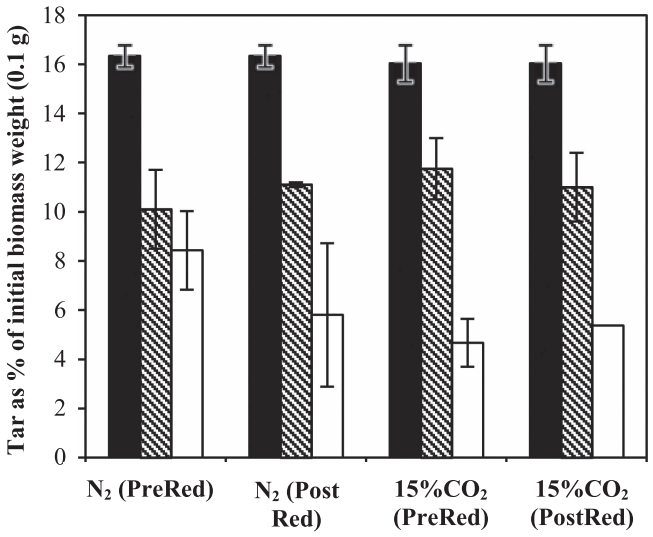

Figure 3. Comparison of the tar yields produced after exposure to the sand beds at 973 K under the different inlet gas compositions (filled bars) and simulated CLC experiments in which the 100Fe(S) OCM (pattern filled) and 60Fe40Al OCM (empty bars) was exposed to volatile pyrolysis products during the 3rd cycle reduction phase at 973 K.

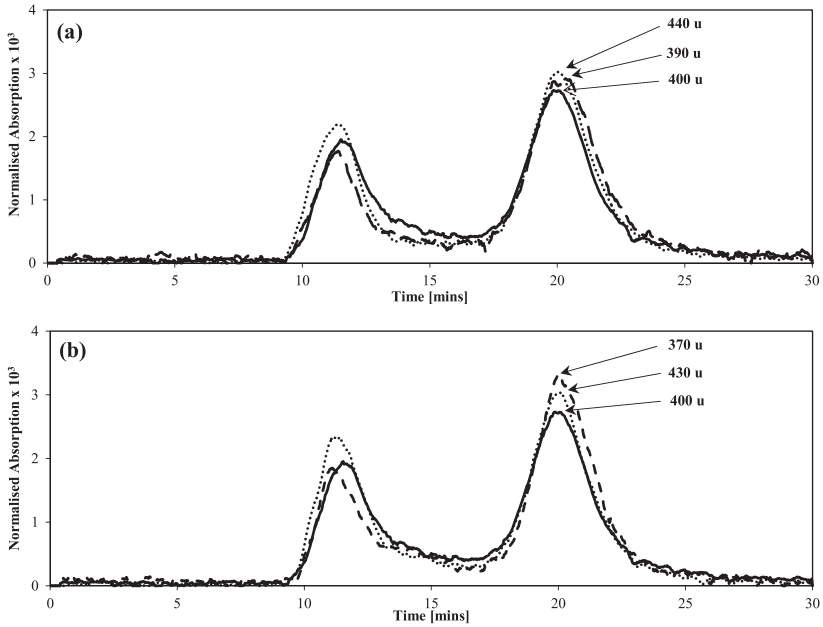

Figure 4. SEC analyses of the tar recovered from the fast pyrolysis of 0.100 g of beech wood in the two-stage reactor loaded with (a) the 100Fe OCM and (b) 60Fe40Al OCM in both their oxidised and reduced forms under a N_2 atmosphere. Sand (——); 'PreRed' conditions (– – –); 'PostRed' conditions (·····).

OCM may have had a small influence on the mechanism by which tar compounds crack and/or reform on the surface of the materials.

The conditions under which the OCMs were exposed to the volatile biomass pyrolysis products (i.e. oxidation state of the OCMs, and inlet gas composition) had a significant effect on the CO_2 and CO yields (figure 5). The CO_2 yields were substantially larger when the OCMs were exposed to the biomass pyrolysis products in their oxidised forms (i.e. experiments denoted as N_2_PreRed and 15%CO_2_PreRed), as would be expected if pyrolysis produces were being oxidised and in turn reducing Fe_2–O_3 to Fe_3O_4.

The yield of CO_2 with the 100Fe OCM during the N_2_PreRed experiments (i.e. which started with Fe_2O_3/final oxidation state not thermodynamically constrained/more CO_2 produced) was slightly higher at 40.9 wt% compared with the 15%CO_2_Pre-Red experiments where the CO_2 yield was 37.1 wt% (reduction of Fe_2O_3 constrained to Fe_3O_4/more unreacted CO present/less CO_2 produced). CO yields were consistent with this, and the 60Fe40Al OCM

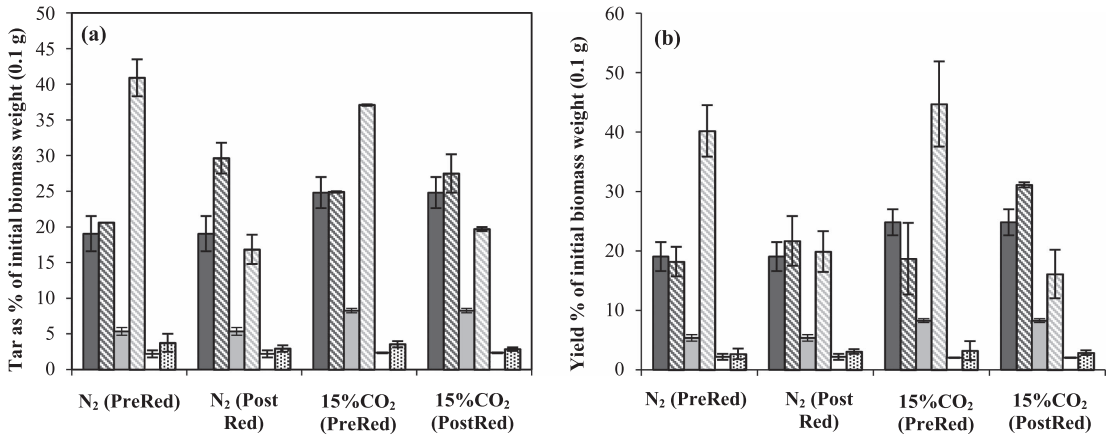

Figure 5. Detectable gas yields produced after the biomass pyrolysis products were exposed to (a) 100Fe OCM (pattern filled bars) and (b) 60Fe40Al OCM (pattern filled bars) compared with the gas yields obtained after exposure to the sand beds (filled bars) at 973 K under the different inlet gas compositions. CO (dark grey bars), CO_2 (light grey bars) and CH_4 (white/polka dot filled bars).

displayed a similar trend, though with a slightly higher overall conversion. This may be because Fe_3O_4 can be further reduced to $FeAl_2O_4$ (which was not supressed by the inclusion of 15 mol% CO_2 in the carrier gas, see figure S.2).

Exposure of the volatile pyrolysis products to the OCMs in their reduced forms (PostRed experiments) produced less CO_2 and more CO than when the OCMs were exposed to the volatile pyrolysis products in their oxidised forms but both the CO_2 and CO yields were higher than those for equivalent experiments with an inert sand bed. More CO was produced in the post reduction experiments with the 100Fe OCM in an atmosphere of 100% N_2 compared with an atmosphere containing 15 mol% CO_2. The additional CO_2 produced was around the same for both the system which was thermodynamically constrained to remain as Fe_3O_4 (i.e. with 15 mol% CO_2 in the inlet gas) and that which was not (i.e. 100% N_2 in the inlet gas). This indicates that reactions of Fe_3O_4 and FeO with pyrolysis products (except CO) to produce CO were fast enough to appreciably occur. The thermodynamic constraint imposed on the 100Fe OC system by the inclusion of 15 mol% CO_2 in the inlet gas meant that the increased yields of CO_2 and CO relative to the equivalent experiments with a 2nd stage sand bed could only have been a result of enhanced cracking and/or gasification of the pyrolysis products on the surface of the reduced 100Fe (Fe_3O_4) OCM.

As mentioned above, the reduction of the 60Fe40Al OCM was not thermodynamically limited to Fe_3O_4 by the introduction of 15 mol% CO_2 in the inlet gas. The increased CO yield could therefore have been the result of either: (i) interactions between the pyrolysis products and the OCM in its less reactive reduced state (Fe_3O_4 and possible $FeAl_2O_4$) resulting in a larger proportion of incomplete, partial oxidation reactions taking place and/or; (ii) enhanced cracking and gasification of the pyrolysis products during experiments carried out with a carrier gas of 15 mol-% CO_2.

Interestingly, the pyrolysis product yields obtained after exposure to the 60Fe40Al OCM were similar to the equivalent yields obtained after exposure to the 100Fe OCM despite the fact that the total amount of the active OC component Fe_2O_3 added to the reactor was lower in the case of the experiments involving the 60Fe40Al OCM. The higher tar eliminating efficacy of the 60Fe40Al OCM was most likely a result of: (i) increased contact between the OCM and pyrolysis products due to the higher surface area of the material (table 2); (ii) improved reactivity of the 60Fe40Al OCM and/or; (iii) the improved oxygen transport capacity due to the ability of the OCM to interact with the support allowing for further reduction of Fe_3O_4 to $FeAl_2O_4$. It has been reported elsewhere in the literature that the presence of Al_2O_3 enhances the reduction reactivity of Fe_3O_4 with CO allowing the formation of $FeAl_2O_4$ compared with the reduction reactivity of Fe_3O_4 in the absence of Al_2O_3 where only $Fe_{0.97}O$ can be formed [45].

Methane yields were low and remained fairly constant between 2.7 and 3.5 wt%. The yields were not affected by the introduction of either OCM relative to the experiments in which the 2nd reactor stage contained an inert sand bed.

The OCMs retrieved after exposure to the pyrolysis products in the 3rd reduction cycle were coated with a thin layer of black carbon (figure S.4). The observed carbon deposition was likely due to thermal/catalytic decomposition of the hydrocarbon species produced during pyrolysis in the first stage on the surface of the OCMs [27]. Small samples of each of the 100Fe and 60Fe40Al OCMs retrieved after exposure to the pyrolysis products were submitted for elemental (CHN) analysis in an attempt to quantify the extents of carbon deposition (table 3).

Table 3. Extent of carbon deposition on the surface of the OCMs retrieved after exposure to the biomass pyrolysis products under the different conditions measured via elemental CHN analysis.

	Carbon content of coked OC (wt%)		Carbon deposition as percentage of initial biomass feed weight (wt%)[a]	
Biomass feed condition	100Fe(S)	60Fe40Al(SAB)	100Fe(S)	60Fe40Al(SAB)
100%N2_Pre-Red	0.53	1.05	3.551	7.35
100%N2_Post-Red	0.82	1.41	5.494	9.87
15%CO2_Pre-Red	<0.3	1.04	—	7.28
15%CO2_Post-Red	0.69	1.28	4.623	8.96
3%CO15%CO2_In-Red	0.4	1.2	2.68	8.4

[a] Assumes that carbon deposition was uniformly distributed across all the surfaces of the OC particles in the 2nd stage reactor bed.

The results of elemental analysis revealed that the extent of carbon deposition was greatest in the case of the 60FeAl OCM compared with the 100Fe OCM (table 3). Carbon deposition on the surface of the particles accounted for 2.7–5.5 wt% and 7.3–9.9 wt% of the initial biomass feed mass for the 100Fe OCM and 60Fe40Al OCM respectively. The increase in carbon deposition observed for the 60Fe40Al OCM compared with the 100Fe OCM was roughly equivalent to the magnitude of the difference between the reductions in the respective tar yields. The extent of carbon deposition was also higher when the OCMs were exposed to the pyrolysis products in their reduced form. These results show that controlling the conversion (or reduction) extent of these Fe-based OCMs as a measure for supressing carbon deposition may not be sufficient on its own when dealing with chemical-looping processes using fuel gases containing large quantities of tar. However, regeneration of the coked OCMs was achieved in a subsequent oxidation period with 10 mol% O_2 and, importantly, no adverse effects on the reactivity of the OCMs in subsequent simulated CLC cycles was observed.

Based on the results reported here, the tar cracking effect of the OCMs appeared to be independent of the oxidation state in which the OCMs were exposed to the volatile biomass pyrolysis products (i.e. Fe_2O_3 or Fe_3O_4). This indicates that the enhanced elimination of tar in the presence of both Fe-based OCMs was due to enhanced thermal or catalytic cracking on the surface of the OCMs rather than the result of tar species directly reacting with the OCM. The increased yields of CO_2 that were observed when the biomass tar was exposed to the OCMs in their oxidised forms was likely due to the oxidation of lighter, previously undetected gaseous hydrocarbons and/or the oxidation of the products produced from the tar cracking interactions that took place on the surface of the OCMs.

Gas yield measurements revealed that exposing the pyrolysis products to the oxidised OCMs resulted in a greater conversion to CO_2 as is desirable in a CLC process. A lower conversion to CO_2 was observed when the pyrolysis products were exposed to the reduced OCMs with interactions appearing to favour production of CO. Conversion of the tar species and other pyrolysis products to CO is particularly desirable for applications of CLR and biomass syngas upgrading.

4. Conclusions

A new 6 kW_e laboratory-scale, two-stage fixed-bed reactor for simulating CLC with *ex situ* solid fuel gasification has been designed and constructed. Studies of the interactions between OCMs consisting of pure iron oxide, and 60 wt% Fe_2O_3 iron oxide supported on Al_2O_3 and a gas stream produced from the pyrolysis of biomass to emulate a fuel gas containing large quantities of tar were carried out. The presence of both OCMs at 973 K was found to significantly reduce the amount of biomass tar by up to 71 wt% in the case of the 60 wt% Fe_2O_3/40 wt% Al_2O_3 OCM compared with experiments conducted with an inert bed.

Exposing the pyrolysis vapours to the OCs in their oxidised form favoured the production of CO_2. The production of CO was favoured when the OCs were in their reduced forms.

Both OCMs were affected by carbon deposition. Carbon deposition was removed in the subsequent oxidation phase with no obvious deleterious effects on the reactivity of the OCMs after exposure to the pyrolysis gases and vapours.

Acknowledgments

The authors wish to thank the EPSRC under the RCUK Energy programme for MBH's PhD studentship and additional funding under EP/I010912/1. Multi-scale evaluation of advanced technologies for capturing the CO_2: chemical-looping applied to solid fuels.

References

[1] Pachauri R K *et al* 2014 *Climate Change 2014: Synthesis Report. Contribution of Working Groups I, II and III to the Fifth Assessment Report of the Intergovernmental Panel on Climate Change* IPCC

[2] Boot-Handford M E *et al* 2014 Carbon capture and storage update *Energy Environ. Sci.* **7** 130

[3] Lyngfelt A, Leckner B and Mattisson T A 2001 Fluidized-bed combustion process with inherent CO_2 separation: application of chemical-looping combustion *Chem. Eng. Sci.* **56** 3101

[4] Lyngfelt A 2011 Oxygen carriers for chemical looping combustion-4000 h of operational experience *Oil Gas Sci. Technol. Revue D IFP Energ. Nouv.* **66** 161

[5] Adánez J, Abad A, García-Labiano F, Gayán P and de Diego L 2012 Progress in chemical-looping combustion and reforming technologies *Progr. Energ. Combust. Sci.* **38** 215

[6] Fan L-S 2011 *Chemical Looping Systems for Fossil Energy Conversions* (New York: Wiley)

[7] Mukherjee S, Kumar P, Yang A and Fennell P 2015 Energy and exergy analysis of chemical looping combustion technology and comparison with pre-combustion and oxy-fuel combustion technologies for CO_2 capture *J. Environ. Chem. Eng.* **3** 2104

[8] Linderholm C, Mattisson T and Lyngfelt A 2009 Long-term integrity testing of spray-dried particles in a 10 kW chemical-looping combustor using natural gas as fuel *Fuel* **88** 2083

[9] Jin H G and Ishida M 2002 Reactivity study on natural-gas-fueled chemical-looping combustion by a fixed-bed reactor *Ind. Eng. Chem. Res.* **41** 4004

[10] Kolbitsch P, Bolhàr-Nordenkampf J, Pröll T and Hofbauer H 2009 Comparison of two Ni-based oxygen carriers for chemical looping combustion of natural gas in 140 kW continuous looping operation *Ind. Eng. Chem. Res.* **48** 5542

[11] Adánez J, Dueso C, de Diego L F, García-Labiano F, Gayán P and Abad A 2009 Methane combustion in a 500 W_{th} chemical-looping combustion system using an impregnated Ni-based oxygen carrier *Energ. Fuels* **23** 130

[12] Anthony E J 2008 Solid looping cycles: a new technology for coal conversion *Ind. Eng. Chem. Res.* **47** 1747

[13] Berguerand N, Lyngfelt A, Mattisson T and Markström P 2011 Chemical looping combustion of solid fuels in a 10 kW_{th} unit *Oil Gas Sci. Technol. Revue D IFP Energ. Nouv.* **66** 181

[14] Dennis J S and Scott S A 2010 *In situ* gasification of a lignite coal and CO_2 separation using chemical looping with a Cu-based oxygen carrier *Fuel* **89** 1623

[15] Leion H, Lyngfelt A and Mattisson T 2009 Solid fuels in chemical-looping combustion using a NiO-based oxygen carrier *Chem. Eng. Res. Des.* **87** 1543

[16] Lyngfelt A 2014 Chemical-looping combustion of solid fuels—status of development *Appl. Energy* **113** 1869

[17] Kim H R *et al* 2013 Coal direct chemical looping combustion process: design and operation of a 25 kW_{th} sub-pilot unit *Fuel* **108** 370

[18] Berguerand N and Lyngfelt A 2009 Chemical-looping combustion of petroleum coke using ilmenite in a 10 kW_{th} unit-high-temperature operation *Energy Fuels* **23** 5257

[19] Wang J S and Anthony E J 2008 Clean combustion of solid fuels *Appl. Energy* **85** 73

[20] Cuadrat A, Linderholm C, Abad A, Lyngfelt A and Adánez J 2011 Influence of limestone addition in a 10 kW_{th} chemical-looping combustion unit operated with petcoke *Energy Fuels* **25** 4818

[21] Li F X, Zeng L A and Fan L S 2010 Biomass direct chemical looping process: process simulation *Fuel* **89** 3773

[22] Shen L, Wu J, Xiao J, Song Q and Xiao R 2009 Chemical-looping combustion of biomass in a 10 kW_{th} reactor with iron oxide as an oxygen carrier *Energy Fuels* **23** 2498

[23] Adánez-Rubio I, Abad A, Gayán P, de Diego L F, García-Labiano F and Adánez J 2014 Biomass combustion with CO_2 capture by chemical looping with oxygen uncoupling (CLOU) *Fuel Process. Technol.* **124** 104

[24] Luo S *et al* 2013 Conversion of woody biomass materials by chemical looping process-kinetics, light tar cracking, and moving bed reactor behavior *Ind. Eng. Chem. Res.* **52** 14116

[25] Mendiara T, Abad A, de Diego L F, García-Labiano F, Gayán P and Adánez J 2013 Biomass combustion in a CLC system using an iron ore as an oxygen carrier *Int. J. Greenh. Gas Control* **19** 322

[26] McGlashan N, Shah N, Caldecott B and Workman M 2012 High-level techno-economic assessment of negative emissions technologies *Process Saf. Environ. Protect.* **90** 501

[27] Mendiara T, Johansen J M, Utrilla R, Geraldo P, Jensen A D and Glarborg P 2011 Evaluation of different oxygen carriers for biomass tar reforming: I. Carbon deposition in experiments with toluene *Fuel* **90** 1049

[28] Corbella B M, De Diego L F, García-Labiano F, Adánez J and Palacios J M 2005 Characterization study and five-cycle tests in a fixed-bed reactor of titania-supported nickel oxide as oxygen carriers for the chemical-looping combustion of methane *Environ. Sci. Technol.* **39** 5796

[29] Thunman H, Lind F, Breitholtz C, Berguerand N and Seemann M 2013 Using an oxygen-carrier as bed material for combustion of biomass in a 12 MW_{th} circulating fluidized-bed boiler *Fuel* **113** 300

[30] Huang Z *et al* 2013 Synthesis gas production from biomass gasification using steam coupling with natural hematite as oxygen carrier *Energy* **53** 244

[31] Keller M, Leion H, Mattisson T and Thunman H 2014 Investigation of natural and synthetic bed materials for their utilization in chemical looping reforming for tar elimination in biomass-derived gasification gas *Energy Fuels* **28** 3833

[32] Larsson A, Israelsson M, Lind F, Seemann M and Thunman H 2014 Using ilmenite to reduce the tar yield in a dual fluidized bed gasification system *Energy Fuels* **28** 2632

[33] Lind F, Seemann M and Thunman H 2011 Continuous catalytic tar reforming of biomass derived raw gas with simultaneous catalyst regeneration *Ind. Eng. Chem. Res.* **50** 11553

[34] Lind F, Berguerand N, Seemann M and Thunman H 2013 Ilmenite and nickel as catalysts for upgrading of raw gas derived from biomass gasification *Energy Fuels* **27** 997

[35] Bolton C, Snape C E, Obrien R J and Kandiyoti R 1987 Influence of carrier gas-flow and heating rates in fixed-bed hydropyrolysis of coal *Fuel* **66** 1413

[36] Monteiro Nunes S, Paterson N, Dugwell D R and Kandiyoti R 2007 Tar formation and destruction in a simulated downdraft, fixed-bed gasifier: reactor design and initial results *Energy Fuels* **21** 3028

[37] Kandiyoti R, Herod A and Bartle K 2006 *Solid Fuels and Heavy Hydrocarbon Liquids: Thermal Characterisation and Analysis* (Amsterdam: Elsevier)

[38] Dabai F, Paterson N, Millan M, Fennell P and Kandiyoti R 2010 Tar formation and destruction in a fixed-bed reactor simulating downdraft gasification: equipment development and characterization of tar-cracking products *Energy Fuels* **24** 4560

[39] Bustamante F *et al* 2005 Uncatalyzed and wall-catalyzed forward water-gas shift reaction kinetics *Aiche J.* **51** 1440

[40] Mattisson T, Lyngfelt A and Cho P 2001 The use of iron oxide as an oxygen carrier in chemical-looping combustion of methane with inherent separation of CO_2 *Fuel* **80** 1953

[41] Bohn C 2010 The production of pure hydrogen with simultaneous capture of carbon dioxide *PhD Thesis* University of Cambridge, UK

[42] Zhang Z 2014 The effect of sulfur on chemical looping combustion with iron oxides *PhD Thesis* Imperial College London, UK

[43] Herod A A, Zhuo Y and Kandiyoti R 2003 Size-exclusion chromatography of large molecules from coal liquids, petroleum residues, soots, biomass tars and humic substances *J. Biochem. Biophys. Methods* **56** 335

[44] Higman C and van der Burgt M 2008 *Gasification* 2nd edn (Oxford: Gulf Professional)

[45] Abad A, García-Labiano F, de Diego L F, Gayán P and Adánez J 2007 Reduction kinetics of Cu-, Ni-, and fe-based oxygen carriers using syngas ($CO + H_2$) for chemical-looping combustion *Energy Fuels* **21** 1843